Journal of Molecular and Cellular Cardiology 130 (2019) 88–95

Contents lists available at ScienceDirect

Journal of Molecular and Cellular Cardiology

journal homepage: www.elsevier.com/locate/yjmcc

Original article

Enhanced closed-state inactivation of mutant cardiac sodium channels (SCN5A N1541D and R1632C) through different mechanisms

Tommy Dharmawan[a,1], Tadashi Nakajima[a,*,1], Takashi Iizuka[a], Shuntaro Tamura[a], Hiroki Matsui[b], Yoshiaki Kaneko[a], Masahiko Kurabayashi[a]

[a] Department of Cardiovascular Medicine, Gunma University Graduate School of Medicine, Maebashi, Gunma, Japan
[b] Department of Laboratory Sciences, Gunma University Graduate School of Health Sciences, Maebashi, Gunma, Japan

ARTICLE INFO

Keywords:
Brugada syndrome
Closed-state inactivation
SCN5A
Sinus node dysfunction
Sodium currents
Supraventricular tachyarrhythmias

ABSTRACT

Background: *SCN5A* variants can be associated with overlapping phenotypes such as Brugada syndrome (BrS), sinus node dysfunction and supraventricular tachyarrhythmias. Our genetic screening of *SCN5A* in 65 consecutive BrS probands revealed two patients with overlapping phenotypes: one carried an *SCN5A* R1632C (in domain IV-segment 4), which we have previously reported, the other carried a novel *SCN5A* N1541D (in domain IV-segment 1).

Objective: We sought to reveal whether or not these variants are associated with the same biophysical defects.

Methods: Wild-type (WT) or mutant SCN5A was expressed in tsA201-cells, and whole-cell sodium currents ($hNa_v1.5/I_{Na}$) were recorded using patch-clamp techniques.

Results: The N1541D-I_{Na} density, when assessed from a holding potential of -150 mV, was not different from WT-I_{Na} as with R1632C-I_{Na}, indicating that SCN5A N1541D did not cause trafficking defects. The steady-state inactivation curve of N1541D-I_{Na} was markedly shifted to hyperpolarizing potentials in comparison to WT-I_{Na} ($V_{1/2}$-WT: –82.3 ± 0.9 mV, n = 15; N1541D: –108.8 ± 1.6 mV, n = 26, P < .01) as with R1632C-I_{Na}. Closed-state inactivation (CSI) was evaluated using prepulses of −90 mV for 1460 ms. Residual N1541D-I_{Na} and R1632C-I_{Na} were markedly reduced in comparison to WT-I_{Na} (WT: 63.8 ± 4.6%, n = 18; N1541D: 15.1 ± 2.3%, n = 19, P < .01 vs WT; R1632C: 5.3 ± 0.5%, n = 15, P < .01 vs WT). Entry into CSI of N1541D-I_{Na} was markedly accelerated, and that of R1632C-I_{Na} was weakly accelerated in comparison to WT-I_{Na} (tau-WT: 65.8 ± 7.4 ms, n = 18; N1541D: 13.7 ± 1.1 ms, n = 19, P < .01 vs WT; R1632C: 39.5 ± 2.9 ms, n = 15, P < .01 vs WT and N1541D). Although N1541D-I_{Na} recovered from closed-state fast inactivation at the same rate as WT-I_{Na}, R1632C-I_{Na} recovered very slowly (tau-WT: 1.90 ± 0.16 ms, n = 10; N1541D: 1.72 ± 0.12 ms, n = 10, P = .41 vs WT; R1632C: 53.0 ± 2.5 ms, n = 14, P < .01 vs WT and N1541D).

Conclusions: Both N1541D-I_{Na} and R1632C-I_{Na} exhibited marked enhancement of CSI, but through different mechanisms. The data provided a novel understanding of the mechanisms of CSI of I_{Na}. Clinically, the enhanced CSI of N1541D-I_{Na} leads to a severe loss-of-function of I_{Na} at voltages near the physiological resting membrane potential (~–90 mV) of cardiac myocytes; this can be attributable to the patient's phenotypic manifestations.

1. Introduction

Brugada Syndrome (BrS) is an inherited arrhythmia disorder characterized by ST-segment elevations in the right precordial leads of a surface electrocardiogram (ECG) and concomitant life-threatening ventricular tachyarrhythmias leading to syncope or sudden death [1,2]. Almost 20% of BrS cases are related to variants in *SCN5A*, which encodes the α-subunit of human cardiac voltage-gated sodium channels/currents ($hNa_v1.5/I_{Na}$) [2,3]. Besides BrS, *SCN5A* variants have also been related to other arrhythmic phenotypes such as sinus node dysfunction (SND) [4,5], supraventricular tachyarrhythmias (SVT) including atrial fibrillation (AF), atrial flutter (AFL) and atrial tachycardia (AT) [6,7], atrioventricular block (AVB) [8,9], and long QT syndrome (LQTS) [10]. These arrhythmic phenotypes can be overlapped by a single *SCN5A* variant.

Hundreds of *SCN5A* variants are reported to be associated with

* Corresponding author at: Department of Cardiovascular Medicine, Gunma University Graduate School of Medicine, 3-39-22 Showa-machi, Maebashi, Gunma 371-8511, Japan.
E-mail address: tnakajim@gunma-u.ac.jp (T. Nakajima).
[1] These two authors contributed equally to this work.

https://doi.org/10.1016/j.yjmcc.2019.03.023
Received 26 December 2018; Received in revised form 27 March 2019; Accepted 29 March 2019
Available online 30 March 2019
0022-2828/ © 2019 Elsevier Ltd. All rights reserved.

these disorders. Most *SCN5A* variants related to BrS cause a loss-of-function of I_{Na} through multiple mechanisms, including defective membrane trafficking, production of non-functional channels, and altered channel gating properties [7,11]. Functional analysis of *SCN5A* variants using patch-clamp techniques can demonstrate novel findings on the structure-function relationships of SCN5A and pathophysiological roles in the clinical phenotypes [7].

Genetic screening of *SCN5A* in 65 consecutive BrS probands revealed two symptomatic probands with overlapping phenotypes, including BrS, SND and SVT. We previously reported the clinical characteristics of one proband carrying an *SCN5A* variant (R1632C) in transmembrane segment 4 (S4) of domain IV (DIV; DIV-S4) of SCN5A, and biophysical defects of the variant [7]. We recently found another proband carrying a novel *SCN5A* variant (N1541D) in transmembrane segment 1 (S1) of DIV (DIV-S1) of SCN5A. Although some pathogenic *SCN5A* variants, including V1532I (associated with type-3 LQTS), have been identified in DIV-S1 [12,13], their biophysical defects have never been examined and the structure-function relationship of SCN5A DIV-S1 remains unclear.

Here we report the clinical characteristics of the *SCN5A* N1541D carrier and the biophysical defects of the variant obtained using whole-cell patch-clamp techniques. Intriguingly, N1541D exhibited a marked hyperpolarizing shift in steady-state inactivation curve, like R1632C [7]. Thus, we investigated the mechanisms underlying the marked hyperpolarizing shift in the steady-state inactivation curves of these two variants.

2. Methods

2.1. Genetic analysis

We analyzed the *SCN5A* in 65 consecutive BrS probands who were referred to us between April 2008 and December 2017. This study was approved by the institutional ethics review board (approval number: 2017-15). Written informed consent for the genetic and functional analyses was obtained from the patient. All coding exons of *SCN5A* (NM_198056.2) and their splice sites were analyzed by the Sanger method as previously described [7].

2.2. Mutagenesis, heterologous expression and cell handling

Mutagenesis, heterologous expression and cell handling were performed as described previously [7]. Briefly, wild-type (WT) human heart sodium channel cDNA α-subunit sub-cloned into pcDNA3.1 vector (hH1-pcDNA3.1) and a plasmid containing β-subunit (pGFP-IRES-hβ1) were provided by Prof. Naomasa Makita (Nagasaki University). Site-directed mutagenesis for *SCN5A* N1541D was constructed using a QuikChange II Site-Directed Mutagenesis Kit (Agilent Technologies, Santa Clara, California). The human kidney cell line tsA-201 was transiently transfected using Lipofectamine 2000 with 0.5 μg of hH1-pcDNA3.1 or 0.5 μg of mutant-pcDNA3.1 in combination with 0.5 μg of pGFP-IRES-hβ1. Transfected tsA-201 cells were maintained as previously described [7].

2.3. Electrophysiological experiments

Membrane sodium currents (I_{Na}) were recorded using whole-cell patch-clamp techniques at room temperature (23–25 °C) as previously described [7]. Briefly, the bath solution for recording membrane currents contained (in mM) 145 NaCl, 4 KCl, 1.8 $CaCl_2$, 1 $MgCl_2$, 10 HEPES, 10 glucose (pH 7.35 with NaOH), and the pipette solution contained (in mM) 10 NaF, 110 CsF, 20 CsCl, 10 EGTA, 10 HEPES (pH 7.35 with CsOH). The electrode resistances were 1.1–2.0 MΩ. Data acquisition was performed using an Axopatch 200B amplifier and pCLAMP10.3 (Molecular Devices, Sunnyvale, CA, USA).

2.4. Data analysis

All pulse protocols are described in figures. Current densities at each test potential were obtained by dividing I_{Na} by cell capacitance. Steady-state activation and steady-state inactivation curves were fitted with Boltzmann functions, time course of fast inactivation was fitted with a single exponential function, and recovery from inactivation was fitted with a double exponential function as previously described [7].

Closed-state inactivation (CSI) was evaluated using a double pulse protocol. Cells were prepulsed to −90 mV for various durations (1–1460 ms) from a holding potential of −150 mV, then stepped to −20 mV to determine the I_{Na} availability following the prepulse. Time course of entry into CSI was fitted with a single exponential function, using Origin software (version 8.1) (OriginLab, Northampton, MA), of the following form: $I(t)/I_{max} = A_0 + A\exp(-t/\tau)$, where A is the amplitude, τ is the time constant, I is the current, and t is the time. Recovery from CSI and recovery from closed-state fast inactivation (CSFI) were evaluated using a double pulse protocol. After applying a prepulse of −90 mV for 500 ms or 20 ms, cells were repolarized to −150 mV for various durations, then stepped to −20 mV to determine I_{Na} availability. Time course of recovery from CSI (after applying a prepulse of −90 mV for 500 ms) was fitted with a double exponential function, using Origin software (version 8.1), of the following form: $I(t)/I_{max} = A_0 + A_f[1-\exp(-t/\tau_f)] + A_s[1-\exp(-t/\tau_s)]$, where A_f and A_s refer to fractional amplitudes of fast and slow components, respectively, and τ_f and τ_s refer to fast and slow components of τ, respectively. Time course of recovery from CSFI (after applying a prepulse of −90 mV for 20 ms) was fitted with a single exponential function, using Origin software (version 8.1), of the following form: $I(t)/I_{max} = A_0 + A[1-\exp(-t/\tau)]$.

2.5. Statistical analysis

All data are expressed as mean ± standard error. The unpaired Student's *t*-test was used to analyze differences. *P* values of < 0.05 were considered to be statistically significant.

3. Results

3.1. Clinical characteristics of a patient with overlapping phenotypes

A 54-year-old male (II-1) (Fig. S1A), who had previously undergone lung cancer surgery, reported feeling faint several times over 10 years. Twelve-lead ECG showed sinus bradycardia (heart rate: 32 bpm) with slight PR prolongation (PR: 206 ms) and slight QRS prolongation (QRS: 106 ms), without QT prolongation (QTc: 387 ms) (Fig. 1A). AFL with 2-to-1 conduction (Fig. 1B) and AF (Fig. 1C), both of which terminated spontaneously, were documented, but he felt no symptoms. Holter ECG showed sinus arrest (Fig. 1D), thus he was diagnosed with SND. Transthoracic echocardiography revealed no structural heart disease. He underwent cavotricuspid isthmus linear ablation, and received a permanent pacemaker. Repeated ECG recordings unveiled spontaneous coved-type ST-segment elevation in lead V2 at the third intercostal space (Fig. 1E), thus he was diagnosed with BrS. The patient's mother (I-2) (Fig. S1A) had received a permanent pacemaker due to SND in her 50s.

3.2. Identification of a novel SCN5A N1541D

Genetic screening of *SCN5A* identified a novel *SCN5A* variant, N1541D (Fig. S1B) in DIV-S1 (Fig. S1C). This variant was not found in the ExAC Browser (http://exac.broadinstitute.org/) and the PolyPhen-2 software program predicted that it was probably damaging (http://genetics.bwh.harvard.edu/pph2/). Thus, it was strongly suggested that the variant was disease-causing. Unfortunately, the patient's family members, including his mother, did not give their consent for a genetic

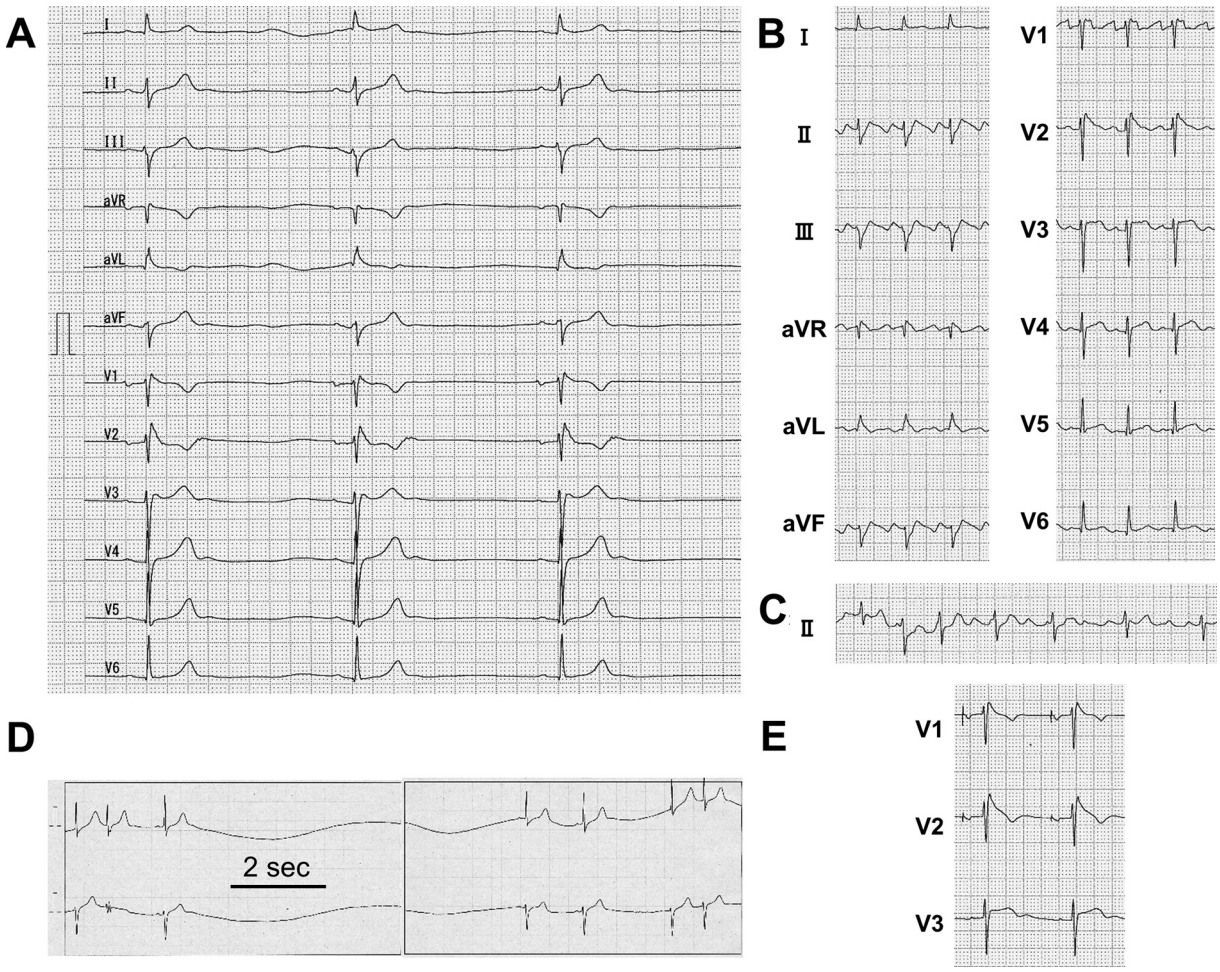

Fig. 1. The overlapping phenotypes of the patient. A: Twelve-lead ECG during sinus bradycardia. B: Twelve-lead ECG during atrial flutter. C: II-lead during atrial fibrillation. D: Holter ECG recording showing sinus arrest. E: Spontaneous coved-type ST segment elevation in a V2-lead at the third intercostal space.

analysis.

3.3. Functional analysis of the SCN5A N1541D

We expressed the wild-type (WT) or the mutant in tsA201 cells in combination with hβ1 subunit, and recorded the whole-cell I_{Na}.

Firstly, pulse protocols were applied from a holding potential of −120 mV. I_{Na} of *SCN5A* N1541D (N1541D-I_{Na}), elicited by various depolarizing test pulses of 20 ms, exhibited a typical I_{Na} resembling the I_{Na} of *SCN5A* WT (WT-I_{Na}) (Fig. 2A). However, the peak N1541D-I_{Na} density, measured at −20 mV, was slightly but significantly smaller than that of WT-I_{Na} (Table 1) (Fig. 2B). The steady-state activation curve of N1541D-I_{Na} was slightly but significantly shifted to hyperpolarizing potentials (~7.6 mV) in comparison to that of WT-I_{Na} (Table 1) (Fig. 2C). The fast inactivation rates of N1541D-I_{Na} were significantly decelerated in comparison to those of WT-I_{Na} at test pulse potentials of below 0 mV (Fig. 2D). Notably, the steady-state inactivation curve of N1541D-I_{Na} was markedly shifted to hyperpolarizing potentials (~26.5 mV) in comparison to that of WT-I_{Na} (Table 1) (Fig. 3A). The fast component of recovery from inactivation of N1541D-I_{Na}, fitted with a double exponential function, was slightly but significantly delayed in comparison to that of WT-I_{Na} (Table 1) (Fig. 3B). Development into intermediate inactivated-state of N1541D-I_{Na}, assessed from a holding potential of −150 mV, was comparable to that of WT-I_{Na} (Fig. 3C).

The marked hyperpolarizing shift in the steady-state inactivation curve of N1541D-I_{Na} suggested that the N1541D-I_{Na} densities elicited by depolarizing test pulses may differ remarkably according to the holding potentials. To confirm this, depolarizing test pulses were applied from various holding potentials (−150 mV, −120 mV and −90 mV) (Fig. S2A, B). The peak N1541D-I_{Na} density, measured at −30 mV from a holding potential of −150 mV, did not differ from that of WT-I_{Na} (WT: −546 ± 35 pA/pF, n = 19; N1541D: -525 ± 64 pA/pF, n = 15, P = .66) (Fig. S2B), indicating that N1541D does not cause trafficking defects. The steady-state activation curve of N1541D-I_{Na} was still shifted to hyperpolarizing potentials (~5.1 mV) in comparison to that of WT-I_{Na} (Fig. S2C). Conversely, the N1541D-I_{Na} density, measured at −20 mV from a holding potential of −90 mV, was remarkably reduced in comparison to that of WT-I_{Na} (WT: −378 ± 35 pA/pF, n = 19; N1541D: –50 ± 14 pA/pF, n = 15, P < .01) (Fig. S2B). These results were consistent with the marked hyperpolarizing shift in the steady-state inactivation curve of N1541D-I_{Na}.

3.4. Closed-state inactivation of the SCN5A N1541D mutation

To reveal the mechanisms underlying the marked hyperpolarizing shift in the steady-state inactivation curve of N1541D-I_{Na}, we examined whether or not the CSI of N1541D-I_{Na} was enhanced. The residual N1541D-I_{Na}, assessed after prepulses of −90 mV for 1460 ms, was markedly reduced in comparison to that of WT-I_{Na} (Table 2) (Fig. 4A, B). Thus, the degree of CSI of N1541D-I_{Na} was markedly enhanced in comparison to WT-I_{Na}. The entry into CSI was fitted with a single exponential function. Intriguingly, the time constant of N1541D-I_{Na} was markedly small in comparison to that of WT-I_{Na} (Table 2). Thus, the entry into CSI of N1541D-I_{Na} was markedly accelerated in comparison

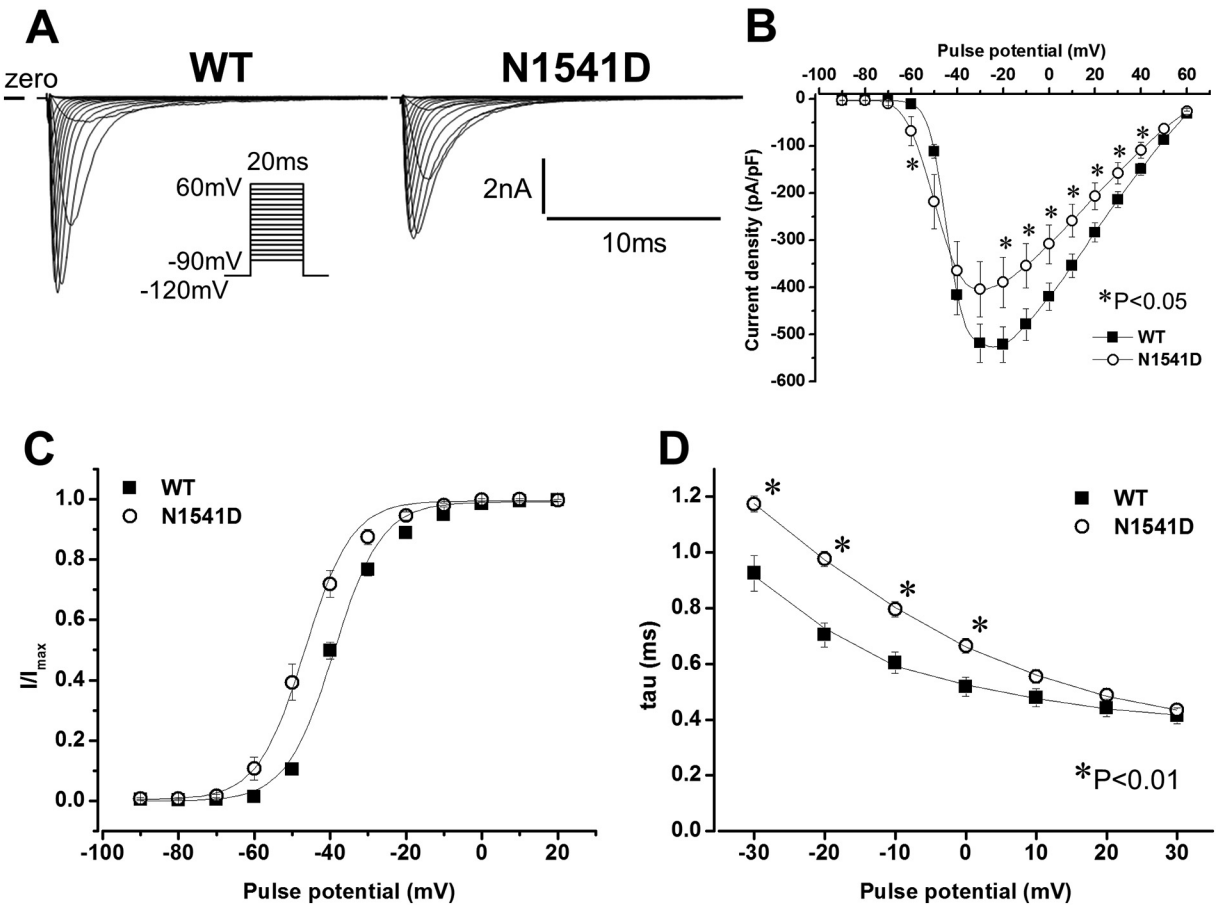

Fig. 2. Expressed sodium currents (I_{Na}) of SCN5A wild-type (WT-I_{Na}) and N1541D (N1541D-I_{Na}), obtained by the activation pulse protocol. A: Representative current tracings of WT-I_{Na} (left) and N1541D-I_{Na} (right). B: Current-voltage relationship of WT-I_{Na} (filled squares, n = 19) and N1541D-I_{Na} (open circles, n = 15). Peak currents obtained by the pulse protocol were normalized to cell capacitances. Asterisks indicate $P < .05$ vs WT-I_{Na}. C: Voltage dependence of activation of WT-I_{Na} (filled squares, n = 19) and N1541D-I_{Na} (open circles, n = 15). Plots were fitted with a Boltzmann function. Fitted data are shown in Table 1. D: Time constants of the voltage dependence of fast inactivation rate of WT-I_{Na} (filled squares, n = 19) and N1541D-I_{Na} (open circles, n = 15). Inactivating currents obtained by the pulse protocol shown in inset A were fitted by a single exponential function. Asterisks indicate $P < .01$ vs WT-I_{Na}.

to WT-I_{Na}.

The recovery from CSI, using a double pulse protocol with a prepulse of −90 mV for 500 ms, and the recovery from CSFI, using a prepulse of −90 mV for 20 ms, were evaluated (Fig. 5A–E). The recovery from CSI was fitted with a double exponential function. The fast and slow time constants of N1541D-I_{Na} were both comparable to those of WT-I_{Na} (Table 2) (Fig. 5A–C). In contrast, the recovery from CSFI was fitted with a single exponential function. The time constant of N1541D-I_{Na} was also comparable to that of WT-I_{Na} (Table 2) (Fig. 5D, E). Thus, N1541D-I_{Na} and WT-I_{Na} rapidly recovered to the same extent from the CSI and CSFI.

3.5. Closed-state inactivation of the SCN5A R1632C mutation

We previously reported that R1632C-I_{Na} also showed a marked hyperpolarizing shift in the steady-state inactivation curve [7]. Therefore, we evaluated the CSI of R1632C-I_{Na} using the same pulse protocol. As with N1541D-I_{Na}, the residual R1632C-I_{Na} was markedly reduced in comparison to that of WT-I_{Na} (Table 2) (Fig. 4A, B). Thus, the CSI of R1632C-I_{Na} was markedly enhanced in comparison to WT-I_{Na}. Although the residual R1632C-I_{Na} was significantly small in comparison to that of N1541D-I_{Na} (Table 2) (Fig. 4B), the time constant of R1632C-I_{Na} was significantly large in comparison to that of N1541D-I_{Na} (Table 2),

Table 1
Parameters of activation, steady-state inactivation and recovery from inactivation.

	Activation			Steady-state inactivation		Recovery from inactivation			
	Current density (pA/pF) at −20 mV	$V_{1/2}$ (mV)	K (mV)	$V_{1/2}$ (mV)	K (mV)	A fast	τ fast (ms)	A slow	τ slow (ms)
WT	−521 ± 38 (n = 19)	−39.1 ± 0.8	6.2 ± 0.3	−82.3 ± 0.9 (n = 15)	5.1 ± 0.2	0.84 ± 0.01 (n = 21)	3.9 ± 0.3	0.16 ± 0.01	38.0 ± 4.0
N1541D	−389 ± 54* (n = 15)	−46.7 ± 1.8†	6.0 ± 0.3	−108.8 ± 1.6† (n = 26)	7.7 ± 0.1†	0.88 ± 0.01† (n = 23)	6.4 ± 0.7†	0.12 ± 0.01†	53.5 ± 6.9

$V_{1/2}$: voltage at which half of the channels are available to open, K: slope factor, A: fractional amplitude, fast: fast component, slow: slow component, T: tau (time constant).

* $P < .05$.

† $P < .01$ vs WT.

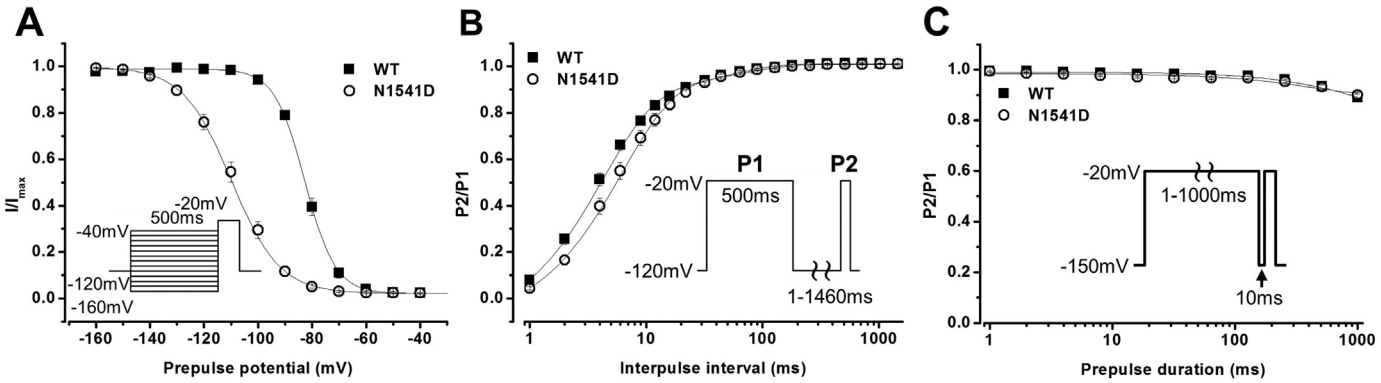

Fig. 3. Steady-state inactivation, recovery from inactivation and development into intermediate inactivated-state of WT-I_{Na} and N1541D-I_{Na}. A: Voltage dependence of steady-state inactivation of WT-I_{Na} (filled squares, n = 15) and N1541D-I_{Na} (open circles, n = 26). Plots were fitted with a Boltzmann function. Fitted data are shown in Table 1. B: Time course of recovery from inactivation of WT-I_{Na} (filled squares, n = 21) and N1541D-I_{Na} (open circles, n = 23). Plots were fitted with a double exponential function. Fitted data are shown in Table 1. C: Development into intermediate inactivated-state of WT-I_{Na} (filled squares, n = 15) and N1541D-I_{Na} (open circles, n = 16). P2/P1 of N1541D-I_{Na} was not different from that of WT-I_{Na} at each prepulse duration.

indicating that the entry into CSI of R1632C-I_{Na} was significantly delayed in comparison to N1541D-I_{Na}, while it was accelerated in comparison to WT-I_{Na}. In contrast, the fast and slow time constants of the recovery from CSI of R1632C-I_{Na} were both remarkably large in comparison to those of WT-I_{Na} and N1541D-I_{Na} (Table 2) (Fig. 5A–C), and the time constant of the recovery from CSFI of R1632C-I_{Na} was also remarkably large in comparison to that of WT-I_{Na} and N1541D-I_{Na} (Table 2) (Fig. 5D, E). Thus, the recoveries from CSI and CSFI of R1632C-I_{Na} were markedly delayed in comparison to those of WT-I_{Na} and N1541D-I_{Na}. While both mutations stabilized CSI, N1541D promoted this effect with accelerated entry, whereas R1632C did so with delayed recovery.

3.6. Activity-dependent loss of I_{Na} availability of the SCN5A N1541D

Since our previous work demonstrated that R1632C-I_{Na} exhibited a marked activity-dependent loss of I_{Na} availability, we examined whether N1541D-I_{Na} exhibits a similar activity-dependent loss of I_{Na} availability using the same pulse protocol (Fig. S3A, B) [7]. When repetitive pulses of 500 ms with cycle lengths of 0.52s were applied, N1541D-I_{Na} exhibited an enhanced activity-dependent loss of I_{Na} availability (Fig. S3A); however, the degree was less than that observed in R1632C-I_{Na}.

4. Discussion

4.1. Biophysical defects of the SCN5A N1541D

We identified a novel *SCN5A* variant (N1541D) in the DIV-S1 of SCN5A in a patient with overlapping phenotypes such as BrS, SND and AFL/AF, and performed a functional analysis. Electrophysiological experiments showed that, although the I_{Na} density of N1541D was significantly reduced in comparison to that of WT when depolarizing test pulses were applied from a holding potential of −120 mV, it did not differ from that of WT when depolarizing test pulses were applied from a holding potential of −150 mV (where the CSI was mostly eliminated), indicating that N1541D did not cause trafficking defects. Despite the absence of trafficking defects, the I_{Na} density of N1541D was markedly reduced and became almost negligible when depolarizing test pulses were applied from a holding potential of −90 mV.

Among several alterations of the channel gating properties of N1541D, the most striking was a marked hyperpolarizing shift in the steady-state inactivation curve. Contrary to R1632C-I_{Na} that also exhibited a marked hyperpolarizing shift in the steady-state inactivation curve [7], N1541D-I_{Na} only showed a slight delay of recovery from inactivation, which might result in a slight enhancement of activity-dependent loss of I_{Na}. The development into intermediate inactivated-state of N1541D-I_{Na} was comparable to that of WT-I_{Na}, although an enhanced intermediate inactivation can be the cause of BrS [14]. The observed hyperpolarizing shift in the activation curve was minimal in comparison to the marked hyperpolarizing shift in steady-state availability, with no window current. While the delay of fast inactivation can theoretically cause a gain-of-function, it remains unclear whether N1541D causes a gain-of-function in physiological conditions.

The degree of residual N1541D-I_{Na} (~15%) in the CSI protocol (Table 2) (Fig. 4B) was close to the N1541D-I_{Na} availability (~12%) assessed at −90 mV in the steady-state inactivation protocol (Fig. 3A) and the peak N1541D-I_{Na} density (~10%) when the holding potential was changed from −150 mV to −90 mV (Fig. S2A, B). These findings indicate that the enhanced CSI of N1541D-I_{Na} is the primary biophysical defect that causes a severe loss-of-function of I_{Na} at voltages near the physiological resting membrane potential (~–90 mV) of cardiac myocytes.

Table 2
Parameters of closed-state inactivation and recovery from closed-state inactivation.

	Closed-state inactivation (−90 mV)			Recovery from closed-state inactivation				Recovery from closed-state fast inactivation
	Residual I_{Na} (%)	τ fast (ms)		A fast	τ fast (ms)	A slow	τ slow (ms)	τ (ms)
WT	63.8 ± 4.6 (n = 18)	65.8 ± 7.4	WT	0.83 ± 0.02 (n = 17)	1.55 ± 0.08	0.17 ± 0.02	26.7 ± 4.3	1.90 ± 0.16
N1541D	15.1 ± 2.3[‡] (n = 19)	13.7 ± 1.1[‡]	N1541D	0.88 ± 0.01[‡] (n = 17)	1.83 ± 0.13	0.12 ± 0.01[‡]	26.5 ± 4.0	1.72 ± 0.12
R1632C	5.3 ± 0.5[‡,‡] (n = 15)	39.5 ± 2.9[‡,‡]	R1632C	0.35 ± 0.04[‡,‡] (n = 13)	13.6 ± 2.6[‡,‡]	0.65 ± 0.04[‡,‡]	76.9 ± 4.4[‡,‡]	53.0 ± 2.5[‡,‡]

[‡] $P < .01$ vs WT.
[‡] $P < .01$ vs N1541D.

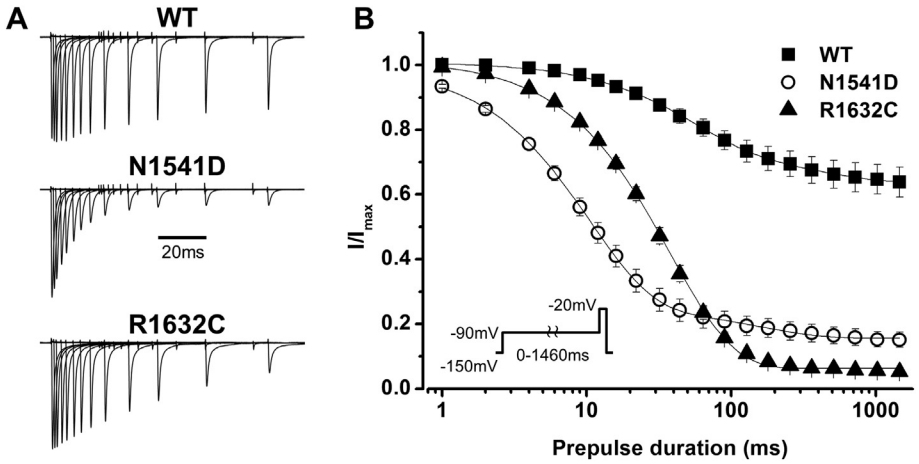

Fig. 4. Closed-state inactivation of WT-I_{Na}, N1541D-I_{Na} and R1632C-I_{Na}. A: Initial 13 representative current tracings of WT-I_{Na} (upper panel), N1541D-I_{Na} (middle panel) and R1632C-I_{Na} (lower panel), obtained by the pulse protocol in inset of B. B: Closed-state inactivation of WT-I_{Na} (filled squares, $n = 18$), N1541D-I_{Na} (open circles, $n = 19$) and R1632C-I_{Na} (filled triangles, $n = 15$), assessed using prepulses of −90 mV for various durations (1–1460 ms). Plots were fitted with a single exponential function. Fitted data are shown in Table 2.

4.2. Enhanced closed-state inactivation of the N1541D-I_{Na} and R1632C-I_{Na} through different mechanisms

The α-subunits of voltage-gated sodium channels (Na_vs) are composed of four homologous but non-identical domains, DI-DIV. Each domain contains an S4 voltage sensor that consists of positively charged amino acid (arginine and lysine) repeats. Sodium channel S4 segments have domain-specific functions, especially in the fast inactivation process [15].

Na_vs can enter into a fast inactivated-state from both open-state(s) (open-state inactivation: OSI) and pre-open closed states (closed-state inactivation: CSI) [16–18]. Upon strong depolarization, voltage sensors (S4 segments) in DI-DIV of Na_vs move outward to promote opening of the activation gate, followed by the binding of the inactivation particle (conserved hydrophobic IFM motif in the cytoplasmic region linking DIII and DIV), resulting in OSI [15,17–21]. Movements of the S4 segments in DI-DIII are requisite for activation gate opening and movement of the S4 segment in DIV is necessary for binding the inactivation particle to its binding sites. Upon weak/subthreshold depolarization, only the S4 segments in DIII and DIV move outward, the activation gate does not open, but this movement is sufficient to allow access of the inactivation particle to its binding sites, resulting in CSI [17,18,20]. Conversely, upon repolarization after inactivation, the S4 segments return to their hyperpolarized position, with a rapid return of the S4 segments in DI and DII and a slow return of the S4 segments in DIII and DIV, which allows the inactivation particle to unbind from its binding sites [17,18,20].

In more detail, the position-specific functions of the first four arginines (R1–R4) in DIV-S4 and putative negative countercharges in the S1-3 segments in the activation and fast inactivation processes have been established [21–23]. Structure-function studies of Na_vs have demonstrated that, in prokaryotic Na_vAb, N25 in S1 forms hydrogen bonds with R105 in S4 in closed-activated conformation [24], and that, in $hNa_v1.4$, N1366 in DIV-S1 (homologous residue to N25 in Na_vAb), one of the residues that may facilitate gating charge transfer, forms hydrogen bonds with R1457 in DIV-S4 (homologous residue to R105 in Na_vAb) [21]. Thus, it is conceivable that, in $hNa_v1.5$, N1541 in DIV-S1 (homologous residue to N1366 in $hNa_v1.4$) also forms a network of hydrogen bonds and interacts with R1632 in DIV-S4 (homologous residue to R1457 in $hNa_v1.4$).

Missense mutations at the first four arginines (Rs) in DIV-S4 in *SCN4A* or *SCN5A* produce significant functional abnormalities related to diverse skeletal or cardiac muscle phenotypes [7,25–32]. When focusing on the fast inactivation process, the main defect of mutations at outer arginines (R1 and R2) in *SCN4A* or *SCN5A* is a delayed fast inactivation [25,26,29,30]. In contrast, that of mutations at central arginines (R3 and R4) is a delayed recovery from inactivation [7,27,28,31]. Of note, a missense mutation at R4 (R1457H) in DIV-S4 in *SCN4A*, found in congenital myasthenic syndrome, produced a marked hyperpolarizing shift in the steady-state availability and a marked delay of recovery from inactivation of $hNa_v1.4$ [28], which resembled the observations in SCN5A R1632C [7]. This supports that each R1-4 in DIV-S4 in *SCN4A* and *SCN5A* has common functional roles in the fast inactivation process. On the other hand, several substitutions of residues in the S1-S3 segments in DIV in the gating charge transfer center have been functionally characterized. Groome et al. [23] reported that N1366D in *SCN4A* produced a hyperpolarizing shift in steady-state availability and delayed recovery from inactivation of $hNa_v1.4$; both were similar to the effects of *SCN5A* N1541D. Intriguingly, Ke et al. [33] reported that N1366S in *SCN4A*, found in paramyotonia congenita, affected both activation and fast inactivation, and disrupted the interaction of N1366S and R1454 in $hNa_v1.4$ at low temperature. Regarding to *SCN5A*, Wang et al. reported that a countercharge mutation (D1595N) in DIV-S3 in the gating charge transfer center exhibited impaired fast inactivation [9,21]. In this study, we demonstrated that the activation curve of N1541D was significantly shifted to hyperpolarizing potentials, similar to the findings of Ke et al. [33] for the paramyotonia congenita mutation N1366S at the homologous residue in $hNa_v1.4$. Moreover, N1541D delayed the entry into OSI and recovery from OSI. Considering the common structure-function relationship of $hNa_v1.4$ and $hNa_v1.5$, the coupling of N1541D with DIV-S4 may be modified in the activation and inactivation processes.

We found that the degree of CSI of N1541D-I_{Na} and R1632C-I_{Na} was markedly enhanced in comparison to WT-I_{Na}. Moreover, the entry into CSI of N1541D-I_{Na} was significantly accelerated in comparison to WT-I_{Na} and R1632C-I_{Na}, and appeared to be the most accelerated among pathogenic *SCN5A* variants such as ΔKPQ [34,35], L1825P [36], E1053K [37] and 1795insD [34], although R1632C-I_{Na} also significantly, but less severely, accelerated the entry into CSI. On the other hand, the recovery from CSI of N1541D-I_{Na} was comparable to that observed in WT-I_{Na}, whereas that of R1632C-I_{Na} was markedly delayed in comparison to WT-I_{Na} and N1541D-I_{Na}, which is possibly due to an impaired movement of the DIV-S4 voltage sensor during repolarization. It is noteworthy that N1541D markedly accelerated the entry into CSI but did not alter the recovery from CSI, while it delayed the entry into OSI and recovery from OSI. These paradoxical phenomena suggest that the coupling of N1541D with DIV-S4 may be voltage-dependent, and that N1541D markedly affects the coupling in the process of CSI during subthreshold depolarization, but weakly affects it in the process of recovery from CSI during subsequent repolarization.

4.3. Phenotypic manifestations associated with the SCN5A N1541D

Functional analyses revealed that both N1541D and R1632C

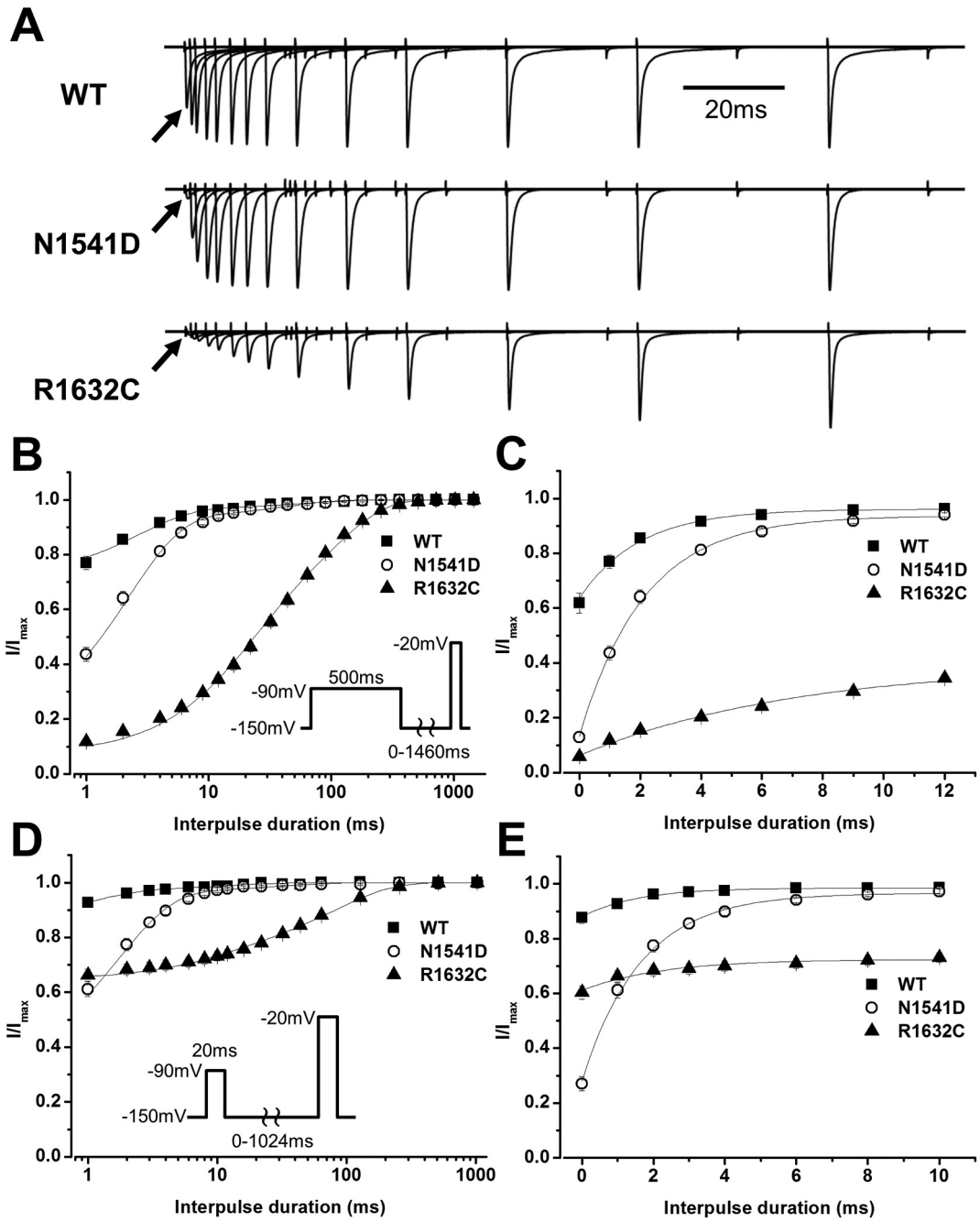

Fig. 5. Recovery from closed-state inactivation and closed-state fast inactivation of WT-I_{Na}, N1541D-I_{Na} and R1632C-I_{Na}. A: Initial 14 representative current tracings of WT-I_{Na} (upper panel), N1541D-I_{Na} (middle panel) and R1632C-I_{Na} (lower panel), obtained by the pulse protocol in inset of B. Arrows indicate the first current tracings (interpulse duration of 0 ms). B: Time course of recovery from closed-state inactivation of WT-I_{Na} (filled squares, n = 17), N1541D-I_{Na} (open circles, n = 17) and R1632C-I_{Na} (filled triangles, n = 13), assessed after various interpulse durations (1–1460 ms) between prepulses of −90 mV for 500 ms and a depolarizing pulse of −20 mV. Plots were fitted with a double exponential function. Fitted data are shown in Table 2. C: Time course of recovery from closed-state inactivation of WT-I_{Na} (filled squares, n = 17), N1541D-I_{Na} (open circles, n = 17) and R1632C-I_{Na} (filled triangles, n = 13), assessed after short interpulse durations (0–12 ms), are shown. During this period, plots were fitted with a single exponential function. Note that WT-I_{Na} and N1541D-I_{Na} rapidly recovered from closed-state inactivation within several milliseconds whereas R1632C-I_{Na} recovered very slowly. D: Time course of recovery from closed-state fast inactivation of WT-I_{Na} (filled squares, n = 10) and N1541D-I_{Na} (open circles, n = 10) and R1632C-I_{Na} (filled triangles, n = 14), assessed after various interpulse durations (1–1024 ms) between prepulses of −90 mV for 20 ms and a depolarizing pulse of −20 mV. Plots were fitted with a single exponential function. Fitted data are shown in Table 2. E: Time course of recovery from closed-state fast inactivation of WT-I_{Na} (filled squares, n = 10), N1541D-I_{Na} (open circles, n = 10) and R1632C-I_{Na} (filled triangles, n = 14), assessed after short interpulse durations (0–10 ms), are shown. During this period, plots were fitted with a single exponential function. Note that WT-I_{Na} and N1541D-I_{Na} rapidly recovered from the closed-state fast inactivation within several milliseconds whereas R1632C-I_{Na} recovered very slowly.

variants caused severe loss-of-function of I_{Na}, without trafficking defects, at voltages near the resting membrane potential of cardiac myocytes. The physiological I_{Na} may consist of the sum of WT-I_{Na} and mutant-I_{Na} because each single subunit can produce a pore-forming channel, therefore it does not cause dominant-effects. All overlapping phenotypes of N1541D or R1632C carrier can be associated with the loss-of-function of I_{Na} in both ventricle and atrium [7]. However, since most pathogenic *SCN5A* variants cause trafficking defects and may

theoretically be associated with overlapping phenotypes, how carriers of *SCN5A* variants that have an enhanced CSI of I_{Na} are specifically associated with overlapping phenotypes should be investigated.

In conclusion, we identified a novel *SCN5A* N1541D variant, in DIV-S1 of SCN5A, in a patient with overlapping phenotypes. N1541D-I_{Na} exhibited a marked hyperpolarizing shift in the steady-state inactivation curve like R1632C-I_{Na}, and both N1541D-I_{Na} and R1632C-I_{Na} exhibited marked enhancement of CSI but through different mechanisms: the entry into CSI was markedly accelerated in N1541D-I_{Na} and weakly accelerated in R1632C-I_{Na}, whereas the recovery from CSI was markedly delayed in R1632C-I_{Na}. These findings provided a novel understanding of the mechanisms of CSI in I_{Na}. Clinically, the enhanced CSI of I_{Na} leads to a severe loss-of-function of I_{Na} at voltages near the physiological resting membrane potential of cardiac myocytes, and may therefore be associated with the patient's phenotypic manifestations.

Acknowledgments

We thank Naomasa Makita, MD, PhD (Nagasaki University) for kindly providing us with hH1 and hβ1 plasmids. We also thank Ms. Takako Kobayashi and Ms. Miki Matsui for their helpful technical assistances.

Funding

This work was supported by a Grant-in-Aid for Scientific Research (C) from the Japan Society for the Promotion of Science (grant number 17K09487 to T.N.).

Disclosures

None.

Appendix A. Supplementary data

Supplementary data to this article can be found online at https://doi.org/10.1016/j.yjmcc.2019.03.023.

References

[1] P. Brugada, J. Brugada, Right bundle branch block, persistent ST segment elevation and sudden cardiac death: a distinct clinical and electrocardiographic syndrome. A multicenter report, J. Am. Coll. Cardiol 20 (1992) 1391–1396.
[2] T. Nakajima, Y. Kaneko, M. Kurabayashi, Unveiling specific triggers and precipitating factors for fatal cardiac events in inherited arrhythmia syndromes, Circ. J. 79 (2015) 1185–1192.
[3] Q. Chen, G.E. Kirsch, D. Zhang, R. Brugada, J. Brugada, P. Brugada, et al., Genetic basis and molecular mechanism for idiopathic ventricular fibrillation, Nature 392 (1998) 293–296.
[4] D.W. Benson, D.W. Wang, M. Dyment, T.K. Knilans, F.A. Fish, M.J. Strieper, et al., Congenital sick sinus syndrome caused by recessive mutations in the cardiac sodium channel gene (SCN5A), J. Clin. Invest. 112 (2003) 1019–1028.
[5] T. Makiyama, M. Akao, K. Tsuji, T. Doi, S. Ohno, K. Takenaka, et al., High risk for bradyarrhythmic complications in patients with Brugada syndrome caused by SCN5A gene mutations, J. Am. Coll. Cardiol. 46 (2005) 2100–2106.
[6] P.T. Ellinor, E.G. Nam, M.A. Shea, D.J. Milan, J.N. Ruskin, C.A. MacRae, Cardiac sodium channel mutation in atrial fibrillation, Heart Rhythm. 5 (2008) 99–105.
[7] T. Nakajima, Y. Kaneko, A. Saito, M. Ota, T. Iijima, M. Kurabayashi, Enhanced fast-inactivated state stability of cardiac sodium channels by a novel voltage sensor SCN5A mutation, R1632C, as a cause of atypical Brugada syndrome, Heart Rhythm. 12 (2015) 2296–2304.
[8] H.L. Tan, M.T. Bink-Boelkens, C.R. Bezzina, P.C. Viswanathan, G.C. Beaufort-Krol, P.J. van Tintelen, et al., A sodium-channel mutation causes isolated cardiac conduction disease, Nature 409 (2001) 1043–1047.
[9] D.W. Wang, P.C. Viswanathan, J.R. Balser, A.L. George Jr., D.W. Benson, Clinical, genetic, and biophysical characterization of SCN5A mutations associated with atrioventricular conduction block, Circulation 105 (2002) 341–346.
[10] P.B. Bennett, K. Yazawa, N. Makita, A.L. George Jr., Molecular mechanism for an inherited cardiac arrhythmia, Nature 376 (1995) 683–685.
[11] T. Zimmer, R. Surber, SCN5A channelopathies–an update on mutations and mechanisms, Prog. Biophys. Mol. Biol. 98 (2008) 120–136.
[12] J.D. Kapplinger, D.J. Tester, B.A. Salisbury, J.L. Carr, C. Harris-Kerr, G.D. Pollevick, et al., Spectrum and prevalence of mutations from the first 2,500 consecutive unrelated patients referred for the FAMILION long QT syndrome genetic test, Heart Rhythm. 6 (2009) 1297–1303.
[13] M. Clerx, J. Heijman, P. Collins, P.G.A. Volders, Predicting changes to I_{Na} from missense mutations in human SCN5A, Sci. Rep. 8 (2018) 12797.
[14] D.W. Wang, N. Makita, A. Kitabatake, J.R. Balser, A.L. George Jr., Enhanced Na(+) channel intermediate inactivation in Brugada syndrome, Circ. Res. 87 (2000) E37–E43.
[15] A. Cha, P.C. Ruben, A.L. George Jr., E. Fujimoto, F. Bezanilla, Voltage sensors in domains III and IV, but not I and II, are immobilized by Na^+ channel fast inactivation, Neuron 22 (1999) 73–87.
[16] J.I. Gillespie, H. Meves, The time course of sodium inactivation in squid giant axons, J. Physiol. 299 (1980) 289–307.
[17] C.M. Armstrong, Na channel inactivation from open and closed states, Proc. Natl. Acad. Sci. U. S. A. 103 (2006) 17991–17996.
[18] J. Groome, F. Lehmann-Horn, B. Holzherr, Open- and closed-state fast inactivation in sodium channels: differential effects of a site-3 anemone toxin, Channels (Austin) 5 (2011) 65–78.
[19] A.L. Goldin, Mechanisms of sodium channel inactivation, Curr. Opin. Neurobiol. 13 (2003) 284–290.
[20] R. Bahring, M. Covarrubias, Mechanisms of closed-state inactivation in voltage-gated ion channels, J. Physiol. 589 (2011) 461–479.
[21] X. Pan, Z. Li, Q. Zhou, H. Shen, K. Wu, X. Huang, et al., Structure of the human voltage-gated sodium channel Nav1.4 in complex with beta1, Science 362 (2018) eaau2486.
[22] N. Yang, A.L. George Jr., R. Horn, Molecular basis of charge movement in voltage-gated sodium channels, Neuron 16 (1996) 113–122.
[23] J.R. Groome, V. Winston, S1-S3 counter charges in the voltage sensor module of a mammalian sodium channel regulate fast inactivation, J. Gen. Physiol 141 (2013) 601–618.
[24] J. Payandeh, T.M. Gamal El-Din, T. Scheuer, N. Zheng, W.A. Catterall, Crystal structure of a voltage-gated sodium channel in two potentially inactivated states, Nature 486 (2012) 135–139.
[25] M.S. Dice, J.L. Abbruzzese, J.T. Wheeler, J.R. Groome, E. Fujimoto, P.C. Ruben, Temperature-sensitive defects in paramyotonia congenita mutants R1448C and T1313M, Muscle Nerve 30 (2004) 277–288.
[26] H. Poulin, P. Gosselin-Badaroudine, S. Vicart, K. Habbout, D. Sternberg, S. Giuliano, et al., Substitutions of the S4DIV R2 residue (R1451) in NaV1.4 lead to complex forms of paramyotonia congenita and periodic paralyses, Sci. Rep. 8 (2018) 2041.
[27] K. Habbout, H. Poulin, F. Rivier, S. Giuliano, D. Sternberg, B. Fontaine, et al., A recessive Nav1.4 mutation underlies congenital myasthenic syndrome with periodic paralysis, Neurology 86 (2016) 161–169.
[28] W.D. Arnold, D.H. Feldman, S. Ramirez, L. He, D. Kassar, A. Quick, et al., Defective fast inactivation recovery of Nav 1.4 in congenital myasthenic syndrome, Ann. Neurol. 77 (2015) 840–850.
[29] N.G. Kambouris, H.B. Nuss, D.C. Johns, G.F. Tomaselli, E. Marban, J.R. Balser, Phenotypic characterization of a novel long-QT syndrome mutation (R1623Q) in the cardiac sodium channel, Circulation 97 (1998) 640–644.
[30] Y. Ruan, N. Liu, R. Bloise, C. Napolitano, S.G. Priori, Gating properties of SCN5A mutations and the response to mexiletine in long-QT syndrome type 3 patients, Circulation 116 (2007) 1137–1144.
[31] Z. Zeng, J. Zhou, Y. Hou, X. Liang, Z. Zhang, X. Xu, et al., Electrophysiological characteristics of a SCN5A voltage sensors mutation R1629Q associated with Brugada syndrome, PLoS One 8 (2013) e78382.
[32] W. Huang, M. Liu, S.F. Yan, N. Yan, Structure-based assessment of disease-related mutations in human voltage-gated sodium channels, Protein Cell 8 (2017) 401–438.
[33] Q. Ke, J. Ye, S. Tang, J. Wang, B. Luo, F. Ji, et al., N1366S mutation of human skeletal muscle sodium channel causes paramyotonia congenita, J. Physiol. 595 (2017) 6837–6850.
[34] P.C. Viswanathan, C.R. Bezzina, A.L. George Jr., D.M. Roden, A.A. Wilde, J.R. Balser, Gating-dependent mechanisms for flecainide action in SCN5A-linked arrhythmia syndromes, Circulation 104 (2001) 1200–1205.
[35] T. Chen, M.F. Sheets, Enhancement of closed-state inactivation in long QT syndrome sodium channel mutation ΔKPQ, Am. J. Physiol. Heart Circ. Physiol. 283 (2002) H966–H975.
[36] N. Makita, M. Horie, T. Nakamura, T. Ai, K. Sasaki, H. Yokoi, et al., Drug-induced long-QT syndrome associated with a subclinical SCN5A mutation, Circulation 106 (2002) 1269–1274.
[37] P.J. Mohler, I. Rivolta, C. Napolitano, G. LeMaillet, S. Lambert, S.G. Priori, et al., Nav1.5 E1053K mutation causing Brugada syndrome blocks binding to ankyrin-G and expression of Nav1.5 on the surface of cardiomyocytes, Proc. Natl. Acad. Sci. U. S. A. 101 (2004) 17533–17538.